


Meshing angles evaluation of silent chain drive by numerical analysis and experimental test

M. Cali  · G. Sequenzia · S. M. Oliveri · G. Fatuzzo

Received: 24 July 2014 / Accepted: 17 June 2015 / Published online: 3 July 2015
© Springer Science+Business Media Dordrecht 2015

Abstract A methodology for integrating the CAD-CAE design of a chain drive system is presented by evaluating meshing angles. The methodology correlates the angles of engagement with transverse vibrations and the tensile force of the chain links, showing that the dynamic behaviour of a chain drive can be significantly improved by fine tuning the meshing angles. An objective parameter was introduced to evaluate divergence from correct meshing. Here the methodology is applied to optimize the timing chain system of a high power V12 quadruple overhead camshaft engine. The reliability of the method relies on multibody modelling all the components and accurate experimental tests. Correlating the experimental measurements provided exact modelling of the contact forces, exact evaluation of stiffness and damping values and precise dynamic modelling of the tensioners and guides. Finally, the dynamic performance of the two different primary stage chain drive layouts were compared.

Keywords Multibody dynamics · Contact force model · Transverse vibration · Tensioner · Chain stiffness · Meshing impact

1 Introduction

Chain drives are commonly used for power transmission in many applications. Chain drives have become increasingly important in the automotive industry mainly due to their ease of installation and maintenance, and their reliability. In some mechanisms, such as the timing systems of high performance engines, the use of chains leads to complex dynamic behaviours due to the high speeds and considerable power involved. Transverse vibrations, tensile forces, fluctuations and incorrect angles of engagement resulting in slipping and impact must be correctly evaluated and controlled. The timing system and valve train generate approximately 20 % of overall engine friction losses, depending on engine speed [1]. The main friction occurs through contact between the chain and sprockets and between the chain and tensioners becoming much greater the more they deviate from correct engagement. The transients are particularly critical during acceleration and deceleration. Under these conditions, the tensioners and guides play a crucial role. It is therefore particularly important to have valid numerical models to correctly predict the dynamic behaviour of such systems.

There are several studies on timing systems in the literature. Some of these [2–7] describe the system's dynamic behaviour with particular focus on modelling elastic and deformable components (tensioners, guides, belts and chains); others [8, 9] study system contacts, in particular between consecutive chain links, between sprockets and chain links and between

M. Cali (✉) · G. Sequenzia · S. M. Oliveri · G. Fatuzzo
Dipartimento di Ingegneria Industriale, Università di Catania, Viale A. Doria 6, 95125 Catania, Italy
e-mail: mcali@dii.unict.it

chain links and tensioners or guides. These two aspects were correlated by Leamy and Wasfy in [10, 11]: the authors developed a dynamic finite-element model that included frictional contacts in a belt drive system. More recently, Čepon and Boltežar [12] presented a model using the absolute nodal coordinate formulation (ANCF). Contact force problems are formulated as a linear complementarity problem (LCP), which takes into account the discontinuous Coulomb friction law. In Čepon et al. [13] presented a method for evaluating stiffness and damping for a flexible multibody model. Experimental studies of sprocket—chain contact are presented in [14]. Other authors identify the contact parameters suitable for the multibody simulation of chain and belt drives [15–19]. The literature shows studies on both roller chains and silent ones. A mathematical model is developed in [20] to calculate the dynamic response of a roller-chain drive working at constant or variable speed. In Pedersen et al. [21, 22] developed a model of a roller-chain drive to simulate and analyse the roller-chain drives of large marine diesel engines. Wang et al. [23] analyzed the meshing process of the double-pitch silent chain drive and also simulated a comparison test between the new double-pitch silent chain and standard silent chain. In a recent study, Feng et al. [24] simulated the dynamic behaviour of a hybrid car silent chain drive system using multibody software, analysing in particular chain tension, meshing impact load and instantaneous transmission ratio at different velocities. Generally, the models in literature study chain transmission conditions between driven and driver sprockets.

In this study, to realistically simulate the complex dynamics of engagement, a multibody model that incorporates valve trains with phasers and timing subsystems was developed. In particular an integrated methodology investigates how a silent chain meshes in the primary timing mechanism connecting the crankshaft sprocket to the idler sprocket in a V12 quadruple overhead cam engine. This model was validated by experimental test, and improved the system by evaluating its meshing angles which provided important data about placing and aligning the tensioners and chain guides.

2 Methods

The main difficulties in simulating chain drives relate to correctly evaluating impacts and contact forces. In

chain drives, meshing is influenced by impulse forces as well as contact friction and damping. Kinematically, the meshing process never occurs precisely. The interdependence between the system dynamics and engagement phenomena causes discontinuity in chain velocity, impacts and vibrations, as studied by Turnbull and Fawcett [25] and Chew [26].

To realistically simulate the complex dynamics of engagement, the authors developed an integrated multibody model from a parametric 3D CAD model of the engine timing chain, using *MSCAdams/Engine* and assembling several subsystems modelled and analyzed in previous studies [2, 15, 27, 28]. In detail, the model incorporates valve trains with phasers and timing subsystems. The multibody model was validated by comparisons with experimental data, and by measuring the angular oscillations on the sprockets. Subsequently, it was used to optimise the primary stage distribution by evaluating the meshing angles between chain and sprockets (see Fig. 1).

2.1 Multibody model of the timing system

In the primary stage of the timing system, a silent chain connects the crankshaft sprocket to the idler sprocket. In the secondary stages, roller chains connect the idler sprocket to the camshaft sprockets. The secondary stages consist of two banks, left and right. A second silent chain connects the crankshaft to the pump control. The system has two hydraulic tensioners, two mechanical tensioners and six fixed guides. Using the discrete model of Veikos and Freudenstein [29], the roller and silent chain were modelled with concentrated parameters (link by link), connecting the link between, in correspondence to the pins, with a 3D general stiffness-damper force (Fig. 2a).

Angular stiffness (around the Z-axis of Fig. 4a) was considered negligible, while transverse and torsional (around the X and Y-axis of Fig. 4a) stiffness and damping were considered infinite. Longitudinal chain stiffness (Fig. 2b) was determined experimentally. Firstly, a static measure of stiffness was obtained for silent and roller link chains (Fig. 3). One sprocket was locked while increasing torque was applied to the other. So, while chain movement remains three-dimensional it is actually reduced to only X–Y shifts.

In the two secondary stage banks, there are two *C121 HCFS Morse TEC* roller link chains, but in this paper we are only describing the primary stage silent

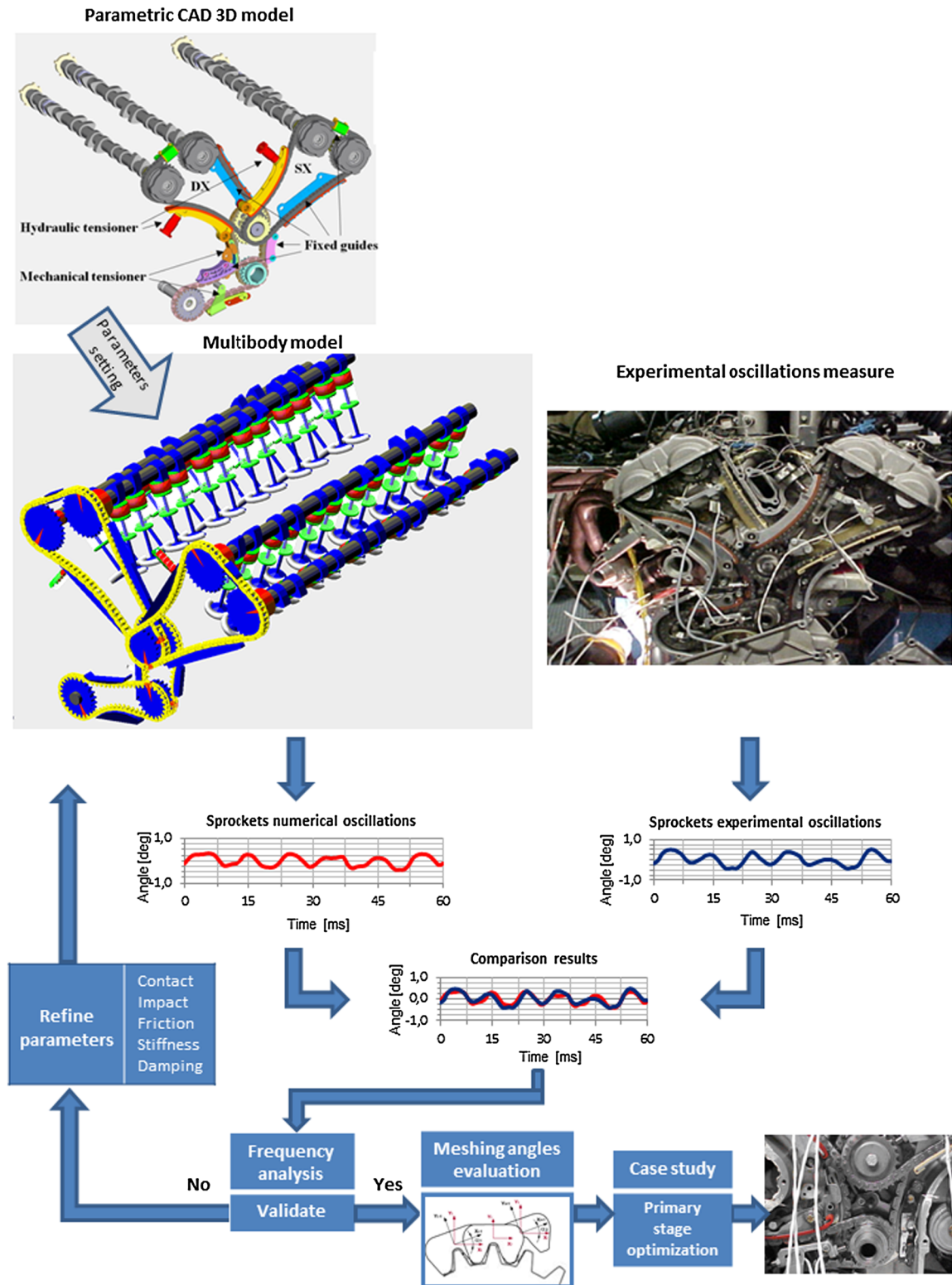


Fig. 1 Summary diagram of the proposed methodology

Fig. 2 General Force (a) and longitudinal stiffness and damping (b) in MBS chain element

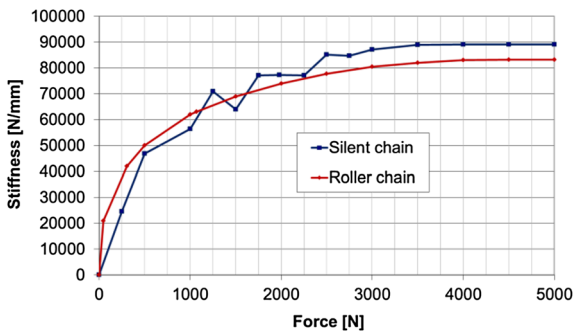
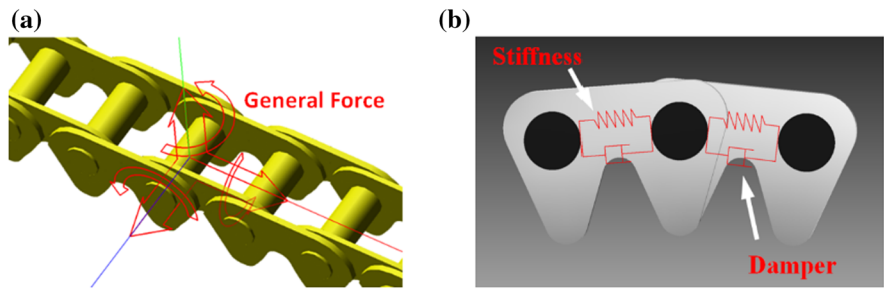


Fig. 3 Longitudinal stiffness in silent and roller chain links

chain, undertaking a thorough analysis of how it engages.

Based on the ANSI standard, silent chain links (Fig. 4a) have plate profiles generated by arcs of circumference and inter-connecting lines defined by six reference points (left and right reference).

The distance between the 0 reference points determines the pitch of the chain which, together with the pressure angle α (inclination of the flanks in the plate profile) (Fig. 4b), is the parameter that most influences meshing.

The sprockets use a standard ISO 606 tooth profile. The profiles of the sprocket tooth flanks were

generated by linking together the involute profile with two arcs of circumference used to model the base and head of the tooth. These profiles were parameterized by introducing: pitch (P); number of teeth (Z); pressure angle (α); Tooth Tip Radius (R_{TT}); Tooth Tip Reference Radius (R_{TTR}); Tooth Root Radius (R_{TR}) and Tooth Root Reference Radius (R_{TRR}). The other four radii shown in Fig. 5, Pitch Radius (R_P), Base Radius (R_B), Root Radius (R_R) and Outer Radius (R_O) combine to determine the tooth geometry and are functions of the previous radii according to the following relations:

Where: $R_P = (P \times Z)/2\pi$, $R_B = R_P - 1.25 P/\pi$, $R_R = R_{TRR} - R_{TR}$, $R_O = R_{TTR} + R_{TT}$.

Table 1 shows the values used to model the profiles in the idler sprockets and silent chain. The involute sprockets have a pressure angle of 20° and pitch length of 9.525 mm. The material's properties and chain contact parameters are shown in Table 2.

In different ways, the hydraulic (Fig. 6) and mechanical (Fig. 7) tensioners dissipate as much vibrational energy as possible, limiting impact and rebound.

In the hydraulic tensioner (Fig. 6a), the forces exchanged between the chain and oscillating plate are regulated by the dynamic behaviour of a piston. The

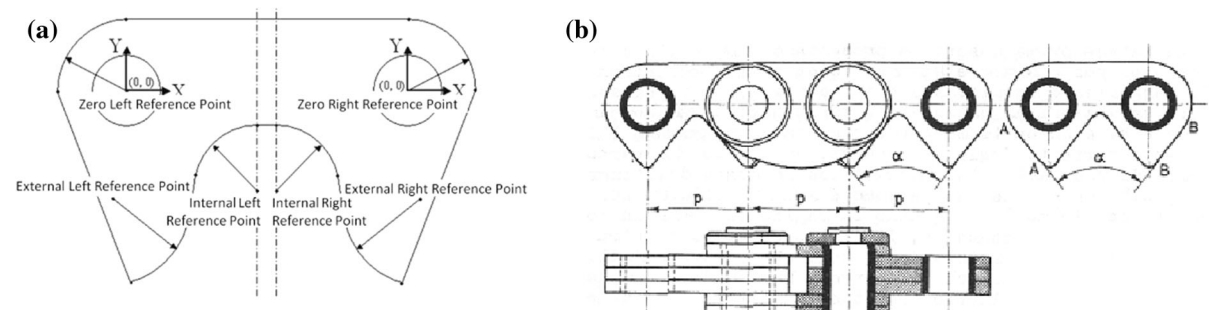


Fig. 4 Plate profile (a) of the ANSI silent chain (b)

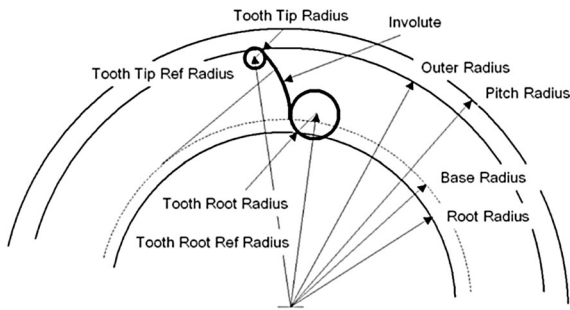


Fig. 5 Geometric parameters in sprocket tooth profile

Table 1 Chain and idler sprocket geometric parameters

Chains plate profile parameters		
Pitch length (P)	9.525 (mm)	
Pressure angle (α)	22°	
Zero radius	4.5 (mm)	
Internal radius	1.6 (mm)	
External radius	2 (mm)	
	X direction (mm)	Y direction (mm)
Zero left reference point	-4.7625	0
Zero right reference point	4.7625	0
Internal left reference point	-0.5	-1.5
Internal right reference point	0.5	-1.5
External left reference point	-5	-1.7
External right reference point	5	-1.7
Idler sprocket profile parameters		
Pitch length (P)	9.525 (mm)	
Pressure angle (α)	22°	
Tooth tip reference radius (RTTR)	44.5 (mm)	
Tooth tip radius (RTT)	1.5 (mm)	
Tooth root reference radius (RTRR)	42.45 (mm)	
Tooth root radius (RTR)	3.27 (mm)	
Pitch radius	42.54 (mm)	

hydraulic tensioner consists of a system of sprung oil chambers (Fig. 6b), in which a piston moves. In the computational model, the hydraulic tensioner force, composed of inertial, hydraulic and elastic components, is given by:

$$F = -m\ddot{s} - c_{eq}\dot{s} - k_m(s - s_0) + pA \tag{1}$$

where m is the translational mass, c_{eq} is the equivalent damping coefficient of the air-oil mixture that takes into account the piston’s permeability, k_m is spring stiffness, s_0 is spring free length, p the pressure in the oil chamber and A the piston cross section. Following the 2nd class lever law, the force on the plate’s contact surface is amplified inversely proportionally to the distance from the rotational pivot. Contact pressure has a linear distribution, with its maximum value at the pivot.

The mechanical tensioners consist of a steel bracket with a pivot pin. A flexible plastic (PA66) blade with two leaf springs rotates around the pivot. To reproduce the variable geometry in the multibody model, the blade was modelled by rigid parts and general forces. When the tensioner recoups the elongation of the chain, it moves outwards and deflects such that the curvature radius of the blade increases. Six fixed guides are installed in the tight spans. Figure 8 shows the three types of fixed guides used in the system’s primary stage (a), secondary stage (b), and oil pump stage (c).

The link-guide contacts are unilateral constraints, as are the link–sprocket contacts. The high number (several hundreds of contacts) involves the resolution of a linear complementarity problem (LCP). To account for the energy dissipation due to impact, friction, vibration and localized deformation during meshing, the non-linear force contact model by Lankarani and Nikravesh [30] was used.

The contact forces that occur during engagement are determined using the *impact function* which applies the Hertz theory to cylindrical surfaces, introducing some corrective measures to deal with the change in stiffness due to the variation in curvature radii. The stiffness coefficients K and K' for the contact between the link and tooth profile and between the link and guides and tensioners are derived using Hertz contact theory. The components in contact are modelled as cylinders made of homogeneous elastic material. The model takes into account the tangential friction forces between the contacts.

The numerical/experimental correlation (Sect. 2.2) established the appropriate level of damping to correctly predict resonance amplitude and verify that it would be correctly predicted under different timing drive simulations. Angular and longitudinal chain damping were evaluated by:

Table 2 Material and contact parameters

Materials and contact properties	Silent chain	Roller chain
Pitch length	9.525 (mm)	9.525 (mm)
Mass of chain link	0.01782 kg	0.0162 kg
Mass per length of chain	1.15 kg m ⁻¹	1.02 kg m ⁻¹
Moment of inertia for each chain link	3.8 × 10 ⁻⁷ kg m ²	3.4 × 10 ⁻⁷ kg m ²
Number of chain link	48	96
Initial chain tensions	200–300 N	350–525 N
Yong modulus	2.07 × 10 ¹¹ kg m ⁻²	2.07 × 10 ¹¹ kg m ⁻²
Poisson coefficient	0.3	0.3
Coefficient of restitution	0.71	0.71
Dynamic friction coefficient	0.26	0.26

Fig. 6 Hydraulic tensioner: tensioner plate (a) and multibody model (b)

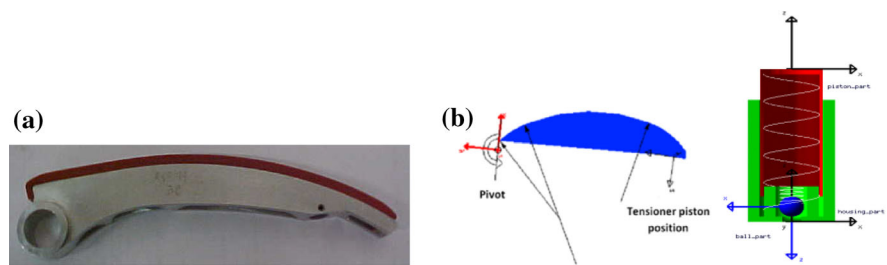


Fig. 7 Mechanical tensioner: components (a) and multibody model (b)

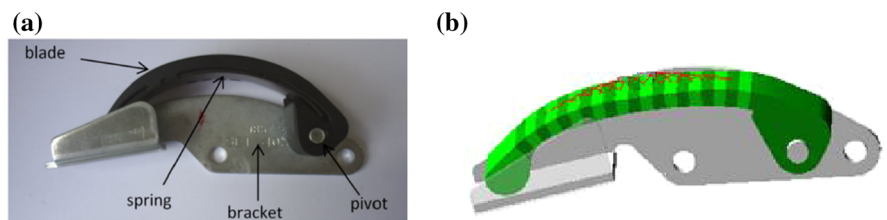


Fig. 8 Fixed guides: in primary stage (a); in secondary stage (b), and in oil pump stage (c)

$$2\zeta = \frac{\omega_1 - \omega_2}{\omega_n} \tag{2}$$

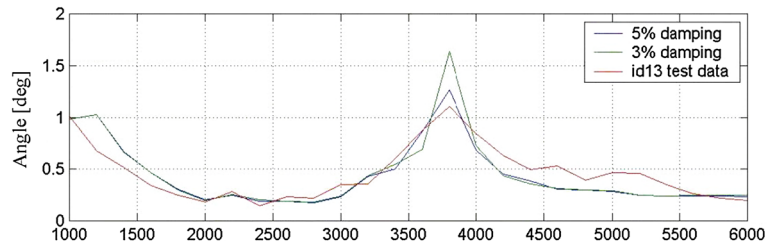
where ζ is the proportion of critical damping, ω_n is the resonant speed and ω_1 and ω_2 are the speeds where the amplitude is $1/\sqrt{2}$ of the resonant amplitude at ω_n .

Figure 9 compares the 3rd order displacement results. From these, the 5 % chain hysteresis damping was chosen as the most appropriate.

The complete model of the timing chain drive consisted of 296 chain links, 7 sprockets and 10 guides, thus many hundreds of contacts and 1800 DOF.

The C++ HHT [31] integrator method was used to integrate the second order differential algebraic equations (DAE). The chain drive model is very sensitive to the integration scheme. The solution error

Fig. 9 Comparison of damping coefficients



must be managed carefully to avoid high oscillations of no interest or unwanted oscillations that are a by-product of the finite element discretization process.

2.2 Model validation

To validate the numerical model the results were compared with the experimental ones from the manufacturer. The angular velocity and oscillation in six driven sprockets and in one driver sprocket were measured in firing condition with 2981A—CCLD Laser Tacho probe Brüel & Kjær precise optical encoders. The numerical and experimental results were compared using two different initial chain tensions (200 and 300 N) and several driver sprocket angular velocities at constant speed (1000, 4000 and 7750 rpm) and during sweep acceleration.

The initial chain span tension was set by changing the mid-distance of the hydraulic tensioner. Based on angular oscillation, it is possible to deduce the natural frequencies for the given operational conditions. Experimental oscillation order tracking showed that 0.5 and 1.5 engine orders (Fig. 10) predominated. In particular, with the idler at 5000 rpm, the 1.5 engine order clearly resonates with the first Eigen frequency.

It was demonstrated that the chain drive mechanism is not influenced much by other engine components and, therefore, only the following reaction torques were applied to the model: those in the camshaft sprockets and that from the oil pump in the pump sprocket. The reaction torques on the camshaft sprocket were evaluated with high precision as a result of the exact modelling of the camshaft with phasers, inlet and exhaust valve train, and oil pump. The driving angular velocity of the crankshaft sprocket took into account the following considerations:

- chain drive behaviour is not periodic within one revolution of the crankshaft or camshaft which is because angular periodic velocity cannot be used to reproduce experimental angular velocity;

- a sweep simulation was used when comparing the experimental data. This reproduces a gradual increase in the angular engine velocity in a given time with constant oscillation.

In this case-study, sweep was set at 1000–8000 rpm in 1.4 s. This does not exactly reflect fire-impulse crankshaft behaviour moderated by the flywheel, but does reproduce resonance oscillation. Driving angular velocity, in phase with the 1.5 engine order, was applied to the crankshaft sprocket using the function given in the appendix. It is possible to observe the response of the system to forcing from the crankshaft and the camshaft. Figure 11 shows the comparison of numerical and experimental angular oscillations of the idler sprocket in an angular range of 1440° (4 laps) at speeds of 4000 and 7750 rpm. The experimental oscillation signal frequencies of the sprockets compare well with the numerical ones (<0.5 % error) with an average quadratic (RMS) signal margin of less than 16 % at all rpm. Figure 11 in particular shows a maximum RMS difference of 15.6 % at 4000 rpm (Fig. 11a) and 15.4 % at 7750 rpm (Fig. 11b) between numerical and experimental oscillations.

Experimentally amplifying the resonance signals can provide 3D general force damping evaluation (paragraph 2.1). The forced analysis highlighted the first resonance frequency of the system at 130 Hz. Figures 12 and 13 show the numerical angular oscillation amplification of the crankshaft sprocket, idler sprocket and camshaft sprocket during resonance.

Resonance at 130 Hz is evident during forcing at both the 1.5 and 3 order. Note that it is evident the relevant correspondence between the oscillations of crankshaft sprocket and idler sprockets (Fig. 14).

Forcing the system, always on the crankshaft sprocket, with a range of 1000–8000 rpm and without oscillatory signal, the effects of the camshaft oscillation on the idler are clear as shown in Fig. 15.

As rpm rose, the system showed a tendency to tune in the resonance. Idler sprocket oscillations are not

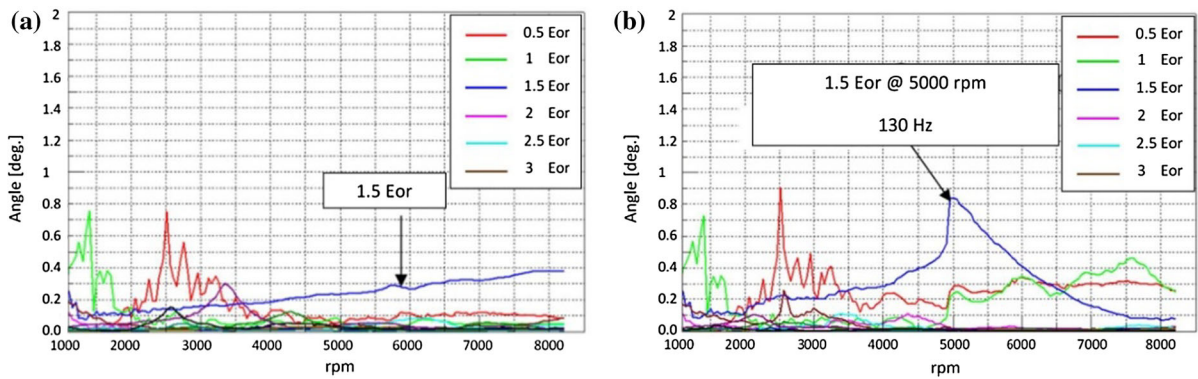
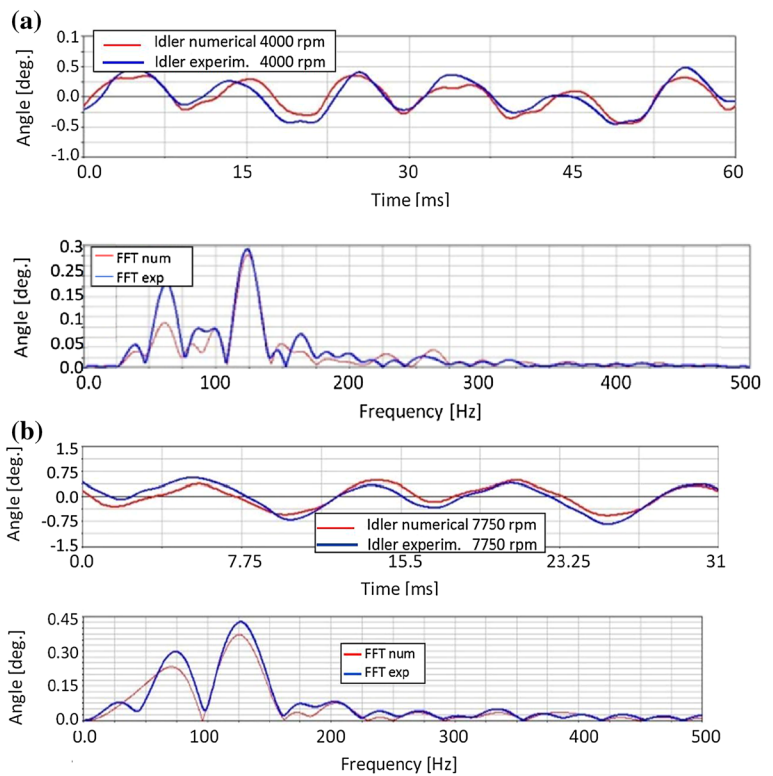


Fig. 10 Experimental order tracking: crankshaft (a) idler (b)

Fig. 11 Experimental and numerical angular oscillations of the idler at 4000 rpm (a) and 7750 rpm (b)



affected by reaction torques from the camshaft until around 5000 rpm. At resonance (7750 rpm), the idler sprocket fluctuates considerably in phase with the camshaft signal as one would expect due to the deformed shape of the first mode in the chain.

The experimental measurements also provided an evaluation of the maximum displacement of the mesh under operating conditions. The values measured (12–15 μm per link) confirm the correctness of the

stiffness values used (Sect. 2.1; Fig. 3) in the multi-body modelling.

3 Meshing angle evaluation

Assuming that ‘correct meshing’ in an ideal plane is where the line of link plate centres is always at a tangent to the primitive circle in the sprocket (circle

Fig. 12 Numerical angular oscillations of crankshaft sprocket, idler sprocket and camshaft sprocket during resonance

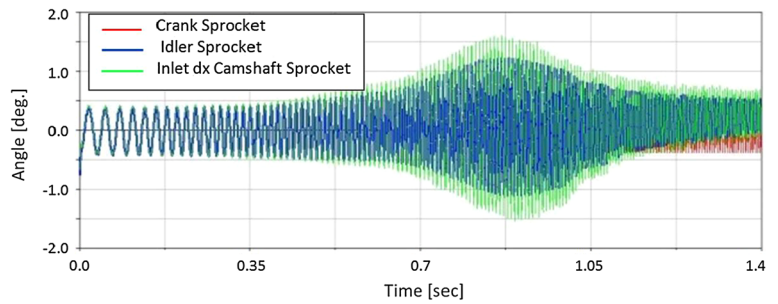


Fig. 13 Numerical angular oscillations and FFT on idler sprocket during resonance (1.5 engine order)

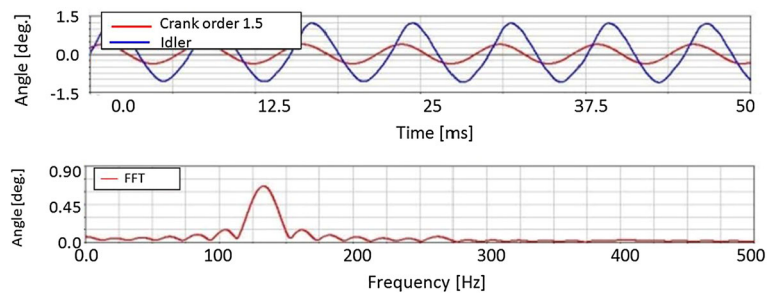


Fig. 14 Numerical angular oscillation on crankshaft and idler sprockets by forcing with 3rd engine order

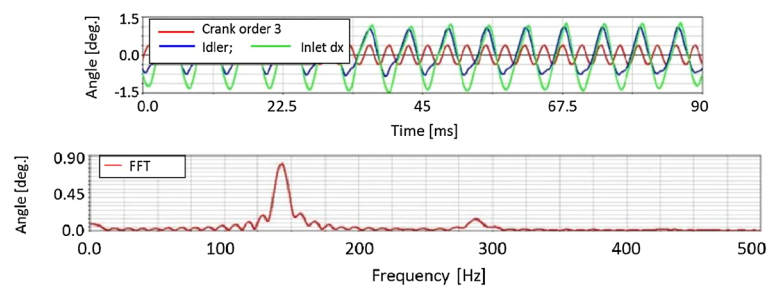
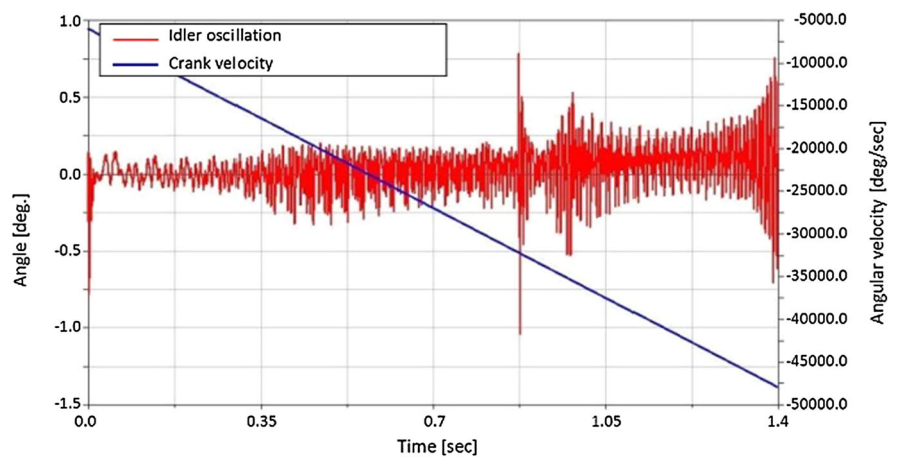


Fig. 15 Idler angular oscillation



that contains the centres of link plates when the links are engaged) (Fig. 16), the indicators of correct meshing would be: the angle α_1 formed by a link engaging with the preceding link and the angle α_2 formed by a link engaging with the one that follows (Fig. 17).

As Fig. 17a shows, the alpha 1 angle measures the relative rotation between the i th link and the previous ($i-1$ th), while the alpha 2 angle measures the relative rotation between the i th link and the following ($i + 1$ th). The alpha 1 and alpha 2 angles are given by:

$$\alpha_1 = \theta_i - \theta_{i-1} \quad (3)$$

$$\alpha_2 = \theta_{i+1} - \theta_i \quad (4)$$

where θ_i is the rotation (anti-clockwise positive) of the i th link around its centre of gravity (Fig. 17b) with respect to tangent direction to the sprocket's primitive circumference and the end of the fixed guide plate.

The alpha 1 and alpha 2 angles of five consecutive links of the chain represent the configuration of a significant length of chain during engagement and disengagement. If the angles are measured again for five consecutive links six times for each chain cycle, chain behaviour can be evaluated accurately during engagement and disengagement. Non-zero alpha angles show irregular meshing with consequent slipping and impact.

The maximum engagement and disengagement angles during transient acceleration described in Sect. 2.2 without any oscillatory signal, were calculated for the first and last contact points on the crankshaft sprocket and idler sprocket. Meshing angles at 1000, 4000 and 7750 rpm are given in Table 3. From the simulation, the gradual stabilization of the angles with increasing angular velocity is clear.

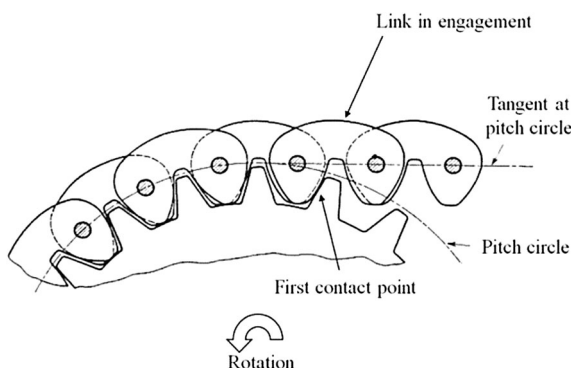


Fig. 16 Regular meshing in silent chain—engaged link

The alpha angles again increase at the resonance speed (7750 rpm), in accordance with Fig. 15.

Although the higher values for the alpha 1 and alpha 2 angles occur (both during short bursts of acceleration and during constant velocity simulations) in the slack span and in particular during the disengaging from the crank sprocket, the most critical phase is still engaging the crank sprocket since the chain is under the greatest traction. Furthermore, the links, no longer controlled by the tensioner, are free to rotate. As they approach the sprocket tooth, they impact significantly on the inside and outside of the tooth (zone A and B in Fig. 18: amplified to highlight the phenomenon).

However, the most critical phase occurs between 1000 and 4000 rpm when they engage with the crankshaft sprocket. At the resonance speed of 7750 rpm, the greatest meshing angles occurred with the idler sprocket. Figure 19 shows the distances between the chain links and the mechanical tensioner surface during resonance (7750 rpm). Two zones can be distinguished: in the first the chain is completely in contact with the tensioner plate; in the second, which accompanies meshing with the idler, the links are not in contact with the surface of the tensioner plate (from 4 to 6.4). This phenomenon is accompanied by transverse vibrations and by incorrect meshing. By evaluating the meshing, the system's dynamic behaviour was optimised without phase changes between the camshaft, valve masses or sprockets and chain size, as outlined in the next sub-section.

3.1 Comparison between two different layouts

As mentioned above, the highest alpha 1 and alpha 2 angles occur always in the slack span and especially on the disengagement from the crank sprocket. Increasing or decreasing angles occur simultaneously during the 4 phases of engagement and disengagement of the crankshaft and triple both during bursts and constant velocity simulations. So, by reducing the alpha angles, the system's dynamic behaviour can be optimized. Furthermore, by using alpha angle engagement analysis, the dynamic performance of two different primary chain drive layouts was compared: *Base* (Fig. 20a) and *Fixed Guide Modified (FGM)* (Fig. 20a). The *Base* model has the traditional layout stage. In the *FGM* an extended and more rigid fixed guide was placed in the tight span.

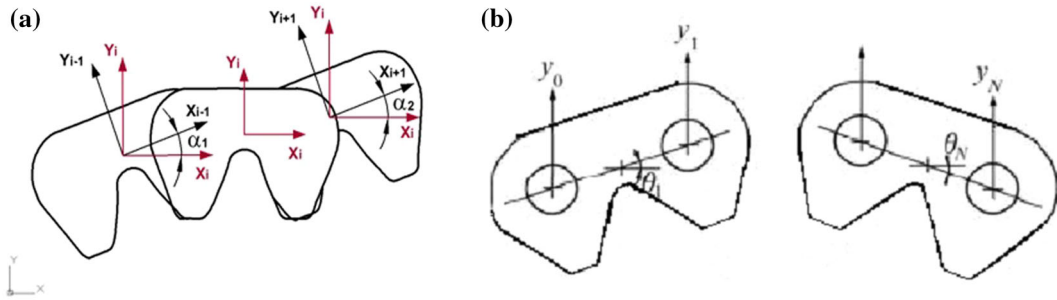
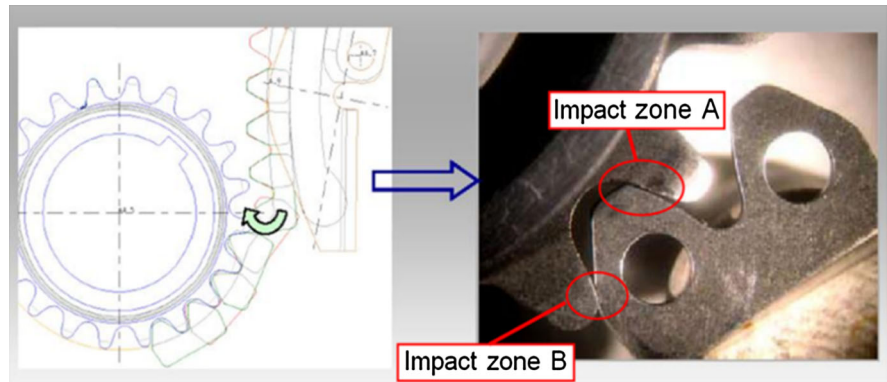


Fig. 17 Meshing angle: rotation of i th link (θ_i) (a) and relative rotation (α_i) (b)

Table 3 Maximum meshing angles in engagement and disengagement on crank sprocket and idler

Angular velocity (rpm)	Position	Time (ms)	α_1 (°)	α_2 (°)
1000	Engaging the crank sprocket	0.00	0.33	0.38
	Disengaging from the crank sprocket	38.08	2.82	2.61
	Engaging the idler	65.08	0.17	0.22
	Disengaging from the idler	117.58	0.53	0.47
4000	Engaging the crank sprocket	615.21	0.21	0.24
	Disengaging from the crank sprocket	624.73	1.76	1.63
	Engaging the idler	631.48	0.11	0.14
	Disengaging from the idler	644.61	0.33	0.35
7750	Engaging the crank sprocket	1377.72	0.48	0.47
	Disengaging from the crank sprocket	1381.23	3.14	3.11
	Engaging the idler	1384.46	0.73	0.75
	Disengaging from the idler	1390.01	0.15	0.13

Fig. 18 Irregular meshing



The high *Base* alpha angle values are due to improper meshing of the chain on the crankshaft sprocket. Moreover, Table 4 shows how the *FGM* mesh angles are lower compared to the *Base* layout which are particularly noticeable in the crank sprocket meshing because the links exiting the fixed guide are

kept very close to the tangent of the primitive circle. As Table 4 and Fig. 20 and 21 show, the *FGM* meshing angles have lower peak RMS and standard deviation (σ) values than the *Base* system.

By analyzing the tensioner spring elongation values in the slack span (Table 5), it can be seen that the

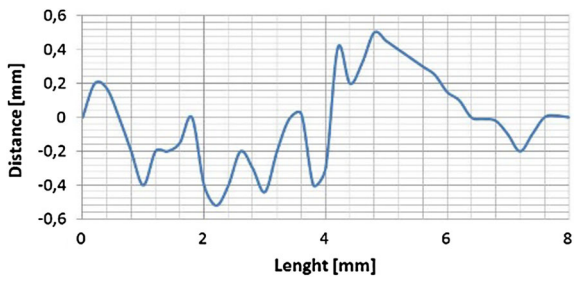


Fig. 19 Link contact with mechanical tensioner

amplitudes are appreciably higher than those of the *FGM* layout which therefore produces a transverse vibration in the chain links all around the chain.

Figure 22 shows the tensile force and transverse vibration in the two layouts at 7750 rpm. The best controlled dynamics of the chain drive are when the length of chain exiting the fixed guide of the output chain driven sprocket is as short as possible (*FGM*

Table 4 Comparing the *Base* and *FGM* layout for engagement on the crank sprocket and idler at 7750 rpm

	<i>Base</i> layout	<i>FGM</i> layout
Engagement on the crank sprocket at 7750 rpm		
α_1		
RMS	7.3°	2.9°
σ	1.14	0.71
α_2		
RMS	3.0°	0.8°
σ	1.32	0.81
Engagement on the idler at 7750 rpm		
α_1		
RMS	2.3°	1.7°
σ	0.55	0.54
α_2		
RMS	0.6°	0.4°
σ	0.60	0.27

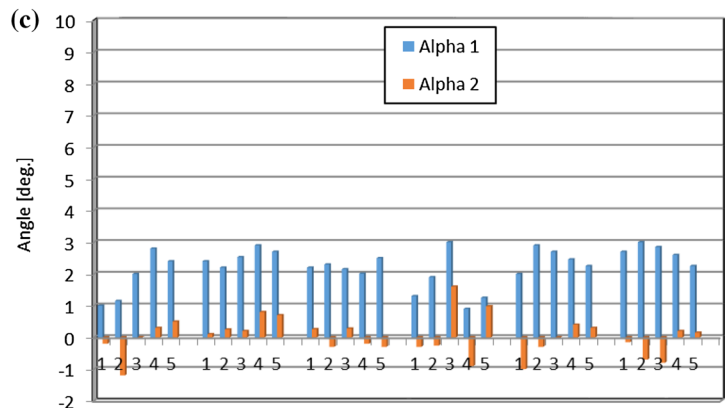
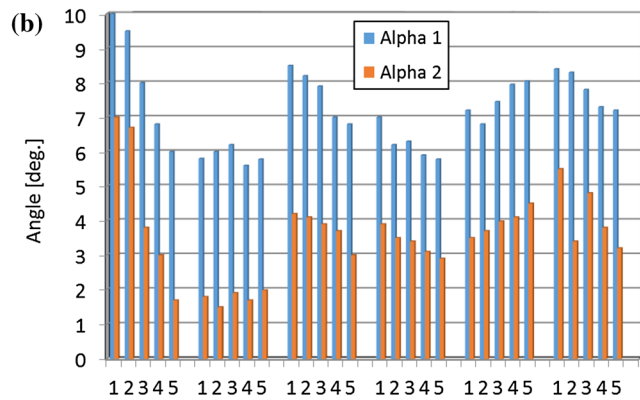
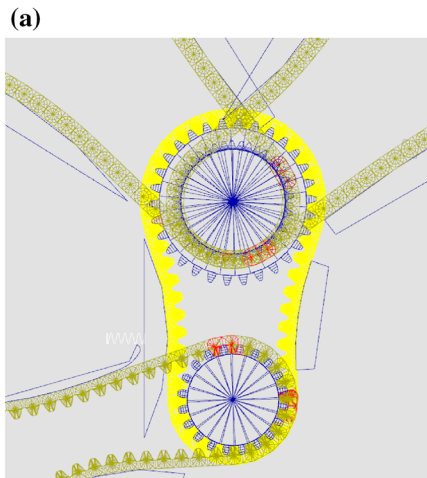


Fig. 20 *Base* layout (a)—Meshing angles on crankshaft sprocket (b) and on idler (c) at 7750 rpm

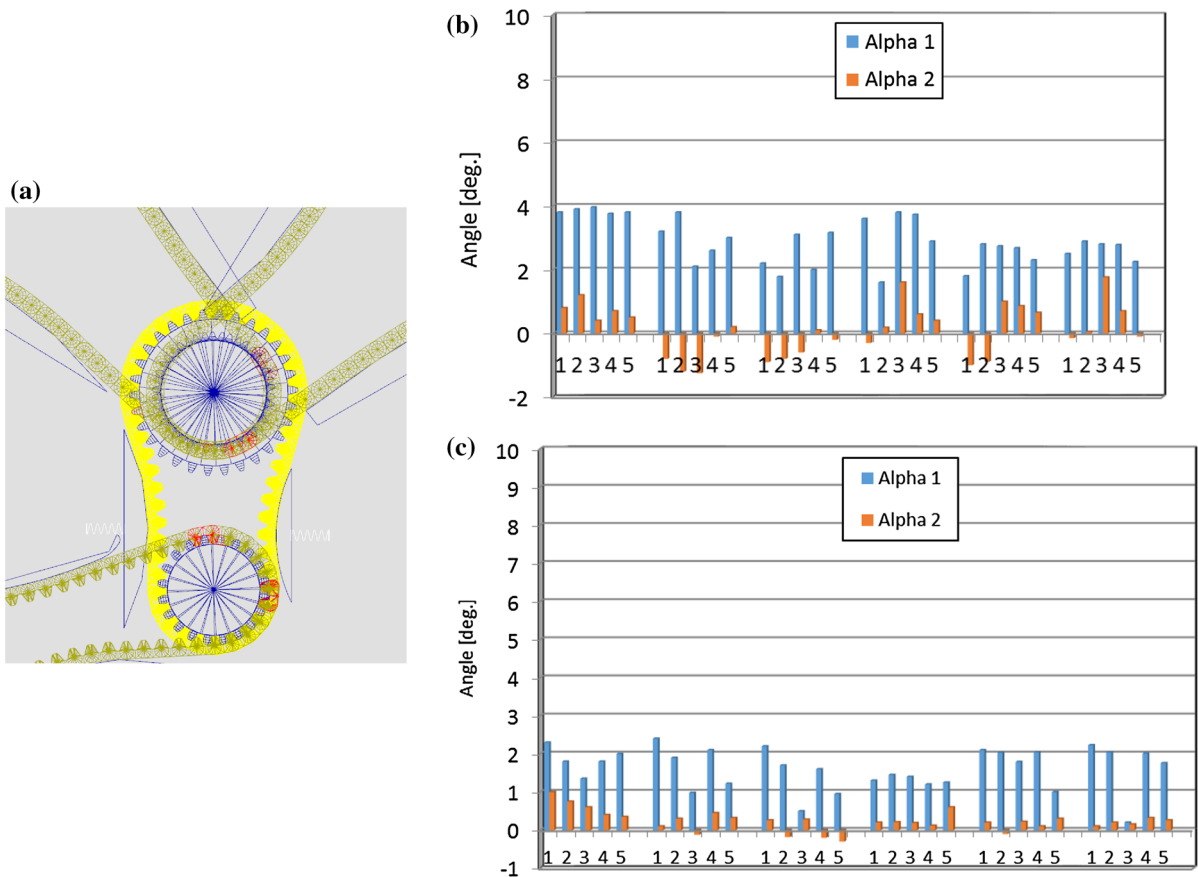


Fig. 21 Fixed guide modified layout (a) Meshing angles on crankshaft sprocket (b) and on idler (c) at 7750 rpm

Table 5 Maximum spring elongation in mechanical tensioner at 7750 rpm

Maximum tensioner spring elongation (mm)	
Base layout	3.48
FGM layout	1.9

layout). Using the alpha angles, the best combination of parameters were found to considerably reduce the loads in the silent chains (Fig. 22a). With slack span accounted for, increased meshing angles cause an increase in the transverse vibration as shown in Fig. 22b, especially in the Base configuration.

Figure 23 shows that between 1000 and 6000 rpm, there are no significant maximum tension differences between the 2 layouts. Over 6000 rpm, especially at the resonance value (7750 rpm), the increase in the Base layout is obvious.

It is therefore clear how appropriate guide configuration gives rise to lower meshing angles thus bringing significant improvements both in terms of tensile force and transverse vibration.

4 Conclusion

The significant importance of meshing angles in dynamically optimising a chain drive system was demonstrated. Usually only the tensile forces, contact forces, angular oscillations and, in some cases, transverse vibrations are used to characterize the dynamic behaviour of chain drive systems. Meshing angles are, however, very important and omitting to evaluate them can lead to serious system dysfunction. This method is effective because it accurately evaluates every structural parameter and exactly models

Fig. 22 Tensile force (a) and transverse vibration (b) in ‘Base’ and ‘FGM’ layout at 7750 rpm

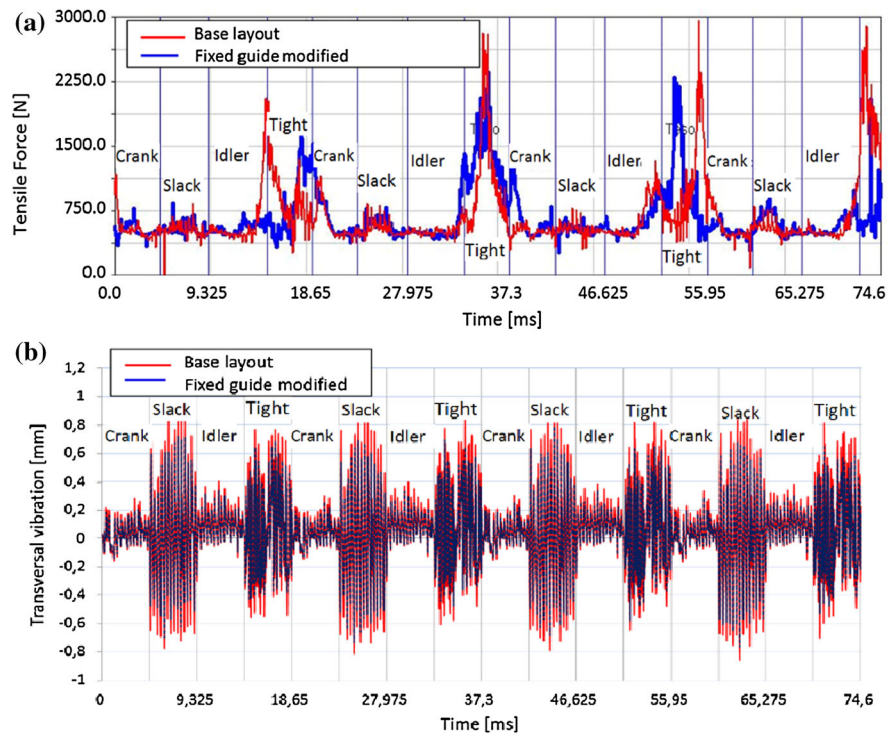
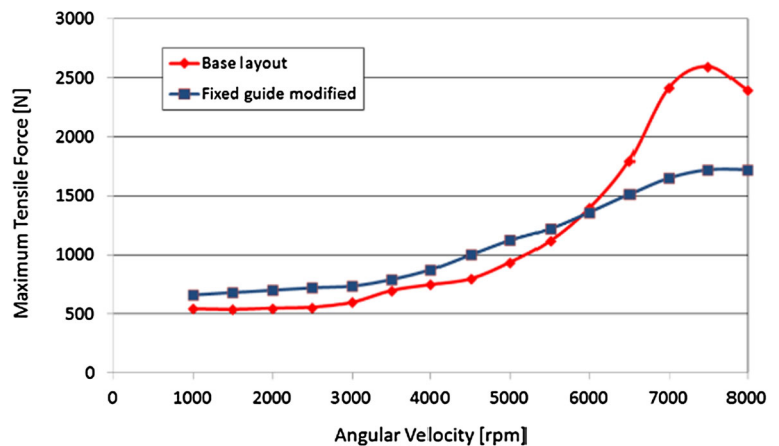


Fig. 23 Maximum tensile force in ‘Base’ and ‘FGM’ layout



within the multibody environment the impact forces of the non-linear contact model proposed by Lankarani and Nikravesh. As a case study, the primary timing chain drive system of a V12 high-performance engine was improved. By analyzing the frequency response of the system and measuring meshing angles under various operating conditions, the dynamic performances of two different chain drive layouts were

compared and an objective parameter was introduced to evaluate divergence from correct meshing. The methodology is suitable for general use in chain drive systems with different chain types and layouts.

Acknowledgments The authors would like to thank ex-director of the Ferrari S.p.A powertrain R&D Eng. Agostino Dominici.

Appendix

FUNCTION = $-6000d \times (1 + 5 \times \text{time}) + 60d \times (1 + 5 \times \text{time}) \times \sin (314 \times (1 + 2.5 \times \text{time}) \times \text{time})$.

References

- Belmer S, Fink T, Lorenz I, Neukirchner H (2005) Timing drives for internal combustion engines. *MTZ Worldwide* 66(6):18–21
- Calì M, Oliveri SM (2001) Numeric and experimental analysis of an engine timing system. In: *Proceeding of the 16th European Mechanical Dynamics Users' Conference*, paper no. 01A18
- Novotný P, Píštěk V (2009) Virtual prototype of timing chain drive. *Eng Mech* 16(2):123–130
- Oliveri SM, Sequenzia G, Calì M (2009) Flexible multibody model of desmodromic timing system. *Mech Based Design Struct Mach* 37(1):15–30
- Zengming F, Kong F, Chengguo D, Fanzhong M (2010) Flexible multi-body contact analysis of rounded-jointed silent chain and sprocket, 5th Asian conference on multi-body dynamics
- Zengming F, Kong F, Chengguo D, Fanzhong M (2010) Flexible multi-body contact analysis of Hy-Vo silent chain and sprocket, 5th Asian conference on Multibody Dynamics
- Čepón G, Boltežar M, Manin L (2011) Validation of a flexible multibody belt-drive model. *J Mech Eng* 57:539–546
- Pereira C, Ambrósio J, Ramalho A (2010) Influence of contact modeling on the dynamics of chain drives, ECCM
- Pereira C, Ambrósio J, Ramalho A (2010) Contact mechanics in a roller chain drive using a multibody approach, 11th Pan-American congress of applied mechanics
- Leamy MJ, Wasfy TM (2002) Transient and steady-state dynamic finite element modeling of belt-drives. *J Dyn Syst Meas Contr* 124:575–581
- Leamy MJ, Wasfy TM (2005) Time accurate finite element modelling of the transient, steady state and frequency responses of serpentine and timing beltdrives. *Int J Veh Des* 39:272–297
- Čepón G, Boltežar M (2009) Dynamics of a belt-drive system using a linear complementarity problem for the belt-pulley contact description. *J Sound Vib* 319:1019–1035
- Čepón G, Manin L, Boltežar M (2009) Introduction of damping into the flexible multibody belt-drive model: a numerical and experimental investigation. *J Sound Vib* 324:283–296
- Sun W, Liu X, Liu J (2012) Inside and Outside Flank Alternate Meshing Silent Chain and Experimental Evaluation of Dynamic Performance. *Res J Appl Sci Eng Technol* 4(7):851–855
- Sequenzia G, Calì M, Oliveri SM (2013) Experimental methodology for the tappet characterization of timing system in I.C.E. *Meccanica* 48(3):753–764
- Hippmann G, Arnold M, Schittenhelm M (2005) Efficient simulation of bush and roller chain drives. In: *Proceedings of the ECCOMAS thematic conference on advances in computational multibody dynamics*
- Pereira C, Ramalho A, Ambrósio J (2011) A critical overview of internal and external cylinder contact force models. *Nonlinear Dyn* 63(4):681–697
- Johnson KL (1987) *Contact mechanics*. Cambridge University Press, Cambridge
- Čepón G, Manin L, Boltežar M (2010) Experimental identification of the contact parameters between a V-ribbed belt and pulley. *Mech Mach Theory* 45:1424–1433
- Xu L, Yang Y, Chang Z, Liu J (2010) Dynamic modeling of a roller chain drive system considering the flexibility of input shaft. *Chin J Mech Eng* 23(3):367–374
- Pedersen SL, Hansen JM, Ambrósio JA (2004) A roller chain drive model including contact with guide-bars. *Multibody Sys Dyn* 12(3):285–301
- Pedersen SL (2005) Model of contact between rollers and sprockets in chain-drive systems. *Arch Appl Mech* 74(7):489–508
- Wang W, Liu X, Liu J, Liu J (2012) Design and experimental analysis of new double-pitch rocker-pin silent chain for conveyors. *Res J Appl Sci Eng Technol* 4(20):4187–4191
- Feng Z, Li J, Liu G (2013) Dynamic analysis of silent chain drive system for hybrid car. *Adv Mater Res* 694–697:84–89
- Turnbull SR, Fawcett JN (1972) Dynamic behaviour of roller chain drives. *Mech Instit Mech Eng* 29–35
- Chew M (1985) Inertia effects of a roller-chain on impact intensity. *J Mech Trans Autom Design, ASME Trans* 107:123–130
- Calì M, Oliveri SM, Sequenzi, G (2007) In: *Proceedings of the IMAC geometric modelling and modal stress formulation for flexible multibody dynamic analysis of crankshaft 25th*
- Sequenzia G, Oliveri S, Calabretta M, Fatuzzo G, Calì M (2011) A new methodology for calculating and modelling non-linear springs in the valve train of internal combustion engines, SAE technical paper. (No. 2011-01-0780)
- Veikos NM, Freudenstein F (1992) On the dynamic analysis of roller chain drives: part 1- theory, In *22nd Biennial Mechanisms conference*. 431–439
- Lankarani HM, Nikravesh PE (1994) Continuous contact force models for impact analysis in multibody systems. *Nonlinear Dyn* 5:193–207
- Hilbert HM, Huges TJR, Taylor RL (1977) Improved numerical dissipation for time integration algorithms in structural dynamics. *Earthq Eng Struct Dynam* 5(3):283–292